FOUR-WAVE MIXING IN WEYL SEMIMETALS

A Dissertation

by

SULTAN ZUWAIMEL F. ALMUTAIRI

Submitted to the Graduate and Professional School of
Texas A&M University
in partial fulfillment of the requirements for the degree of

DOCTOR OF PHILOSOPHY

Chair of Committee,	Alexey Belyanin
Committee Members,	M. Suhail Zubairy
	Alexei Sokolov
	Christi Madsen
Head of Department,	Grigory Rogachev

December 2021

Major Subject: Physics

ABSTRACT

Weyl semimetals (WSMs) have unusual optical responses originating from unique topological properties of their bulk and surface electron states. Their third-order optical nonlinearity is expected to be very strong, especially at long wavelengths, due to linear dispersion and high Fermi velocity of three-dimensional Weyl fermions. Here we derive the third-order nonlinear optical conductivity of WSMs in the long-wavelength limit and calculate the intensity of the nonlinear four-wave mixing signal as it is transmitted through the WSM film or propagates away from the surface of the material in the reflection geometry. All results are analytic and show the scaling of the signal intensity with variation of all relevant parameters. The nonlinear generation efficiency turns out to be surprisingly high for a lossy material, of the order of several mW per W^3 of the incident pump power. Optimal conditions for maximizing the nonlinear signal are realized in the vicinity of bulk plasma resonance. This indicates that ultrathin WSM films of the order of skin depth in thickness could find applications in compact optoelectronic devices.

DEDICATION

To my family.

ACKNOWLEDGMENTS

First and foremost I am extremely grateful to my advisor and mentor Prof. Alexey Belyanin for his invaluable advice, continuous support, and patience during my PhD study.

I would like also to thank former and present members of the Belyanin group, Qianfan Chen, Ryan Kutayiah, Zhongqu Long, and Yongrui Wang, for the many discussions we had throughout the years.

CONTRIBUTORS AND FUNDING SOURCES

Contributors

This work was supported by a dissertation committee consisting of Professors Alexey Belyanin [advisor/chair], M. Suhail Zubairy, and Alexei Sokolov of the Department of Physics & Astronomy and Professor Christi Madsen of the Department of Electrical & Computer Engineering.

The initial idea for the project presented in this disseration was proposed by Prof. Alexey Belyanin. All other work conducted for the dissertation was completed by the student under the supervision of Prof. Alexey Belyanin.

Funding Sources

Graduate study was supported by a scholarship from King Abdulaziz City for Science and Technology (KACST) in Saudi Arabia and the Saudi Arabian Cultural Mission (SACM) in the United States.

TABLE OF CONTENTS

Page

LIST OF FIGURES

FIGURE Page

1. INTRODUCTION

1.1 Nonlinear Optics

Nonlinear optics is the study of phenomena that happen as a result of the changes of the optical properties of the material by the presence of light. So when an incident electrical field changes the optical properties of the material this process is a nonlinear optical process and the study of all such phenomena is the subject of nonlinear optics. They are nonlinear in the sense that they happen when the material system's response to an applied electrical field depends in a nonlinear way upon the strength of the electrical field[1]. It is believed that the field of nonlinear optics was started experimentally with Franken and his co-workers' paper in 1961. Their paper was a milestone where they produced the second harmonics in ultraviolet by shining a red light from ruby laser into quartz doubling its frequency[2]. Although there are claims about nonlinear experiments much earlier but they weren't as significant as Franken's experiment. N. Bloembergen was shown a preprint of Franken's paper and after reading it he immediately assembled a team of three people consisting of John Armstrong, Jacques Ducuing, and Peter Pershan. The team worked hard every day for four months until they produced the monumental 1962 ABDP paper which laid the theoretical foundation for nonlinear optics. Both Franken's experimental discovery and Bloembergen's ABDP paper together started the field of nonlinear optics [3, 4].

To describe accurately what is meant by optical nonlinearity, let's consider the polarization of a material system that depends upon the strength of the applied electrical field at the same point in space $\mathbf{E}(t)$. Here we neglect the spatial dispersion. Polarization is the dipole moment per unit volume. In the conventional linear case which is linear optics, the induced polarization depends linearly upon the electric field strength in a manner described by

$$\mathbf{P} = \chi^{(1)} \cdot \mathbf{E} \tag{1.1}$$

where the constant of proportionality $\chi^{(1)}$ is known as the linear susceptibility. Susceptibilities of

any order are generally a tensor. Moreover, in this form it is valid only for the spectral Fourier harmonics; otherwise the relation becomes an integral over all previous times. Previous relation can be written in a tensor form as

$$\begin{pmatrix} P_x \\ P_y \\ P_z \end{pmatrix} = \begin{bmatrix} \chi_{xx} & \chi_{xy} & \chi_{xz} \\ \chi_{yx} & \chi_{yy} & \chi_{yz} \\ \chi_{zx} & \chi_{zy} & \chi_{zz} \end{bmatrix} \begin{pmatrix} E_x \\ E_y \\ E_z \end{pmatrix} \tag{1.2}$$

In nonlinear optics the optical response is described by generalizing $\mathbf{P} = \chi^{(1)} \cdot \mathbf{E}$ by expressing the polarization as a power series in the field strength as

$$\mathbf{P} = \chi^{(1)} \cdot \mathbf{E} + \chi^{(2)} \cdot \mathbf{EE} + \chi^{(3)} \cdot \mathbf{EEE} + ... = \mathbf{P}^{(1)} + \mathbf{P}^{(NL)} \tag{1.3}$$

where we again have in mind Fourier harmonics of frequency spectrum. The quantities $\chi^{(2)}$ and $\chi^{(3)}$ are known as second and third order nonlinear optical susceptibilities. They are also generally tensors. We shall refer to $\mathbf{P}^{(2)} = \chi^{(2)} \cdot \mathbf{EE}$ and $\mathbf{P}^{(3)} = \chi^{(3)} \cdot \mathbf{EEE}$ as second and third order nonlinear polarization, respectively. It can be shown that second order optical nonlinear interactions can occur only in noncentrosymmetric crystals which are crystals that do not display inversion symmetry. On the other hand, third order optical nonlinear interaction can occur for both centrosymmetric and noncentrosymmetric media.

For example, when the incident electric field consists of two frequency harmonics, $\tilde{\mathbf{E}}(t) = \mathbf{E}_1 e^{-i\omega_1 t} + \mathbf{E}_2 e^{-i\omega_2 t} + c.c.$ the complex amplitudes of the second-order nonlinear polarization for

each frequency component are given by

$$\begin{aligned}
\mathbf{P}(2\omega_1) &= \chi^{(2)}{\mathbf{E_1}}^2 \text{ (Second Harmonic Generation)} \\
\mathbf{P}(2\omega_2) &= \chi^{(2)}{\mathbf{E_2}}^2 \text{ (Second Harmonic Generation)} \\
\mathbf{P}(\omega_1+\omega_2) &= 2\chi^{(2)}\mathbf{E_1}\mathbf{E_2} \text{ (Sum Frequency Generation)} \\
\mathbf{P}(\omega_1-\omega_2) &= 2\chi^{(2)}\mathbf{E_1}\mathbf{E_2^*} \text{ (Difference Frequency Generation)} \\
\mathbf{P}(0) &= 2\chi^{(2)}(\mathbf{E_1}\mathbf{E_1^*}+\mathbf{E_2}\mathbf{E_2^*}) \text{ (Optical Rectification)}
\end{aligned}$$

We have seen that nonlinearity can cause the polarization of the medium to generate new electromagnetic field with new frequency components not originally there. Here starting with Maxwell's equations that describe the fields generated by the polarization in a medium,

$$\nabla\cdot\mathbf{D} = 4\pi\rho \tag{1.4}$$

$$\nabla\cdot\mathbf{B} = 0 \tag{1.5}$$

$$\nabla\times\mathbf{E} = -\frac{1}{c}\frac{\partial\mathbf{B}}{\partial t} \tag{1.6}$$

$$\nabla\times\mathbf{H} = \frac{1}{c}\frac{\partial\mathbf{D}}{\partial t}+\frac{4\pi}{c}\mathbf{J} \tag{1.7}$$

we derive a wave equation that couples nonlinear polarization to the field. We are interested in the region where there are no free charges hence $\rho = 0$ and there is no free current hence $\mathbf{J} = 0$. We also assume the material is nonmagnetic hence $\mathbf{B} = \mathbf{H}$. Moreover, we assume the material is nonlinear in a way that the field $\mathbf{D}$ and $\mathbf{E}$ are related by $\mathbf{D} = \mathbf{E} + 4\pi\mathbf{P}$ where generally the polarization vector $\mathbf{P}$ depends nonlinearly upon the local value of the electric field strength $\mathbf{E}$. By taking the curl of the third Maxwell equation Eq(6) namely $\nabla\times\nabla\times\mathbf{E} = -\frac{1}{c}\frac{\partial\nabla\times\mathbf{B}}{\partial t}$ this can be rewritten as

$$\nabla^2\mathbf{E}-\frac{1}{c^2}\frac{\partial^2\mathbf{E}}{\partial t^2} = \frac{4\pi}{c^2}\frac{\partial^2\mathbf{P}}{\partial t^2} \tag{1.8}$$

Plugging $\mathbf{P} = \mathbf{P}^{(1)}+\mathbf{P}^{(NL)}$ we find this equation

$$\nabla^2\mathbf{E} - \frac{\epsilon}{c^2}\frac{\partial^2\mathbf{E}}{\partial t^2} = \frac{4\pi}{c^2}\frac{\partial^2\mathbf{P}^{(NL)}}{\partial t^2} \tag{1.9}$$

This equation is inhomogeneous and the nonlinear response of the medium represents the source term whereas the linear response is included in the dielectric permittivity and we again assume the monochromatic fields.

After this short and greatly simplified introduction into the nonlinear optics we now turn to four-wave mixing. Four-wave mixing is a nonlinear effect resulting from the third order nonlinearity described by $\chi^{(3)}$. The third order nonlinear polarization will be a function of $\mathbf{E}^3$. When there are incident field components at two input frequencies ω_1 and ω_2, then these two fields can generate the third-order nonlinear polarization at frequencies $\omega_3 = 2\omega_1 - \omega_2$ and $\omega_4 = 2\omega_2 - \omega_1$. In the more general non-degenerate case for the nonlinear polarization at frequency $\omega_n = \pm\omega_1 \pm \omega_2 \pm \omega_3$ there are 8 different combinations of three input frequencies.

Now let us learn how we can mathematically understand this. Three waves incident on a material and one wave coming out can be represented as $\mathbf{E}^{(\omega_n)} = \frac{1}{2}(\mathbf{E}_n e^{i(k_n z - \omega_n t)} + c.c.)$ for each frequency component. Now if we want to know how the new field is generated then we find the nonlinear polarization given by

$$\mathbf{P}^{(NL)} = \chi^{(3)}(\mathbf{E}_1^{(\omega_1)} + \mathbf{E}_2^{(\omega_2)} + \mathbf{E}_3^{(\omega_3)})^3 \tag{1.10}$$

and the nonlinear polarization for example for $\omega_4 = \omega_1 + \omega_2 + \omega_3$ is

$$\mathbf{P}^{(NL_4)} = \frac{6}{8}\chi^{(3)}\mathbf{E_1}\mathbf{E_2}\mathbf{E_3}e^{i((k_1+k_2+k_3)z-\omega_4 t)} \tag{1.11}$$

Typical values of $\chi^{(3)}$ can be found in [1].

1.2 Weyl Semimetals

In 1928, P. A. M. Dirac proposed an equation describing massive spin-1/2 particles in quantum mechanics reconciled with special relativity[5]. The Dirac equation has a 4-component wave

functions and 4×4 matrices. When we take c $= \hbar = 1$, Dirac equation in 3+1D is given by

$$i\partial_t\psi = -i\alpha \cdot \nabla\psi + m\beta\psi \tag{1.12}$$

A year later in 1929, Hermann Weyl apprehended that a real-valued 2-component equation is sufficient to describe massless spin-1/2 particles, splitting the Dirac equation into two parts of different chirality[6]. This equation now is called Weyl equation and it's given by

$$i\partial_t\psi_\pm = \mp\mathbf{p} \cdot \sigma\psi_\pm \tag{1.13}$$

Weyl semimetal is a solid state crystal that lacks either inversion or time reversal symmetry where the low energy quasiparticle excitations correspond to Weyl fermions. In Weyl semimetal, non-degenerate bands touching happens in the three-dimensional momentum space forming linearly dispersed Weyl cones of opposite chiralities. The Hamiltonian of two bands touching at point $\mathbf{k}_0$ and energy ϵ_0 can be expressed as

$$H(\mathbf{k}) = \epsilon_0\sigma_0 \pm \hbar v_F(\mathbf{k} - \mathbf{k}_0) \cdot \sigma \tag{1.14}$$

where σ_0 is the unit matrix, v_F is the Fermi velocity, $\mathbf{k}$ represent the momentum and σ is the Pauli matrix. In the case the touching point of the band set to be zero this Hamiltonian becomes the exact Weyl Hamiltonian. The band crossing is irremovable and robust no matter how we change the parameters.

The topology of Weyl node is understood by the Berry curvature, and to understand that we are going here to derive the Berry phase first and then introduce concepts like Berry curvature and Chern number. My derivation and remaining introduction will follow[7, 8, 9, 10, 11]

The general solution to the time-dependent Schrodinger equation

$$i\hbar\partial_t\Psi(t) = \hat{H}(t)\Psi(t) \tag{1.15}$$

can be written as a linear superposition of the eigenfunctions

$$\Psi(t) = \sum_n \bar{c}_n(t)\psi_n(t) \tag{1.16}$$

If we substitute the general solution Eq.(1.16) into Eq.(1.15) we find

$$i\hbar \sum_n (\dot{\bar{c}}_n\psi_n + \bar{c}_n\dot{\psi}_n) = \sum_n \bar{c}_n E_n \psi_n \tag{1.17}$$

Taking the inner product with ψ_m we obtain

$$\dot{\bar{c}}_m + \sum_n \bar{c}_n \langle\psi_m|\dot{\psi}_n\rangle = -\frac{i}{\hbar}\bar{c}_m E_m \tag{1.18}$$

Let

$$\bar{c}_n(t) = c_n(t)e^{i\theta_n(t)} \tag{1.19}$$

Then

$$\begin{aligned} \dot{c}_m e^{i\theta_m} + i\dot{\theta}_m c_m e^{i\theta_m} + \sum_n c_n e^{i\theta_n}\langle\psi_m|\dot{\psi}_n\rangle &= -\frac{i}{\hbar}c_m e^{i\theta_m}E_m \\ \dot{c}_m + \sum_n c_n e^{i(\theta_n-\theta_m)}\langle\psi_m|\dot{\psi}_n\rangle &= -\frac{i}{\hbar}(\hbar\dot{\theta}_m + E_m)c_m \end{aligned} \tag{1.20}$$

By setting

$$\begin{aligned} \dot{\theta}_m(t) &= -\frac{1}{\hbar}E_m(t) \\ \theta_m(t) &= -\frac{1}{\hbar}\int_0^t E_m(t')dt' \end{aligned} \tag{1.21}$$

So

$$\dot{c}_m = -c_m\langle\psi_m|\dot{\psi}_m\rangle - \sum_{n\neq m} c_n e^{i(\theta_n-\theta_m)}\langle\psi_m|\dot{\psi}_n\rangle \tag{1.22}$$

To find another expression for $\langle\psi_m|\dot{\psi}_n\rangle$ we differentiate Schrodinger equation with respect to time

$$\dot{\hat{H}}\psi_n + \hat{H}\dot{\psi}_n = \dot{E}\psi_n + E\dot{\psi}_n \tag{1.23}$$

We again take the inner product with ψ_m to obtain

$$\langle\psi_m|\dot{\hat{H}}|\psi_n\rangle + \langle\psi_m|\hat{H}|\dot{\psi}_n\rangle = \dot{E}_n\delta_{nm} + E_n\langle\psi_m|\dot{\psi}_n\rangle \tag{1.24}$$

Selecting only the $n \neq m$ terms gives

$$\langle\psi_m|\dot{\psi}_n\rangle = \frac{\langle\psi_m|\dot{\hat{H}}|\psi_n\rangle}{E_n - E_m} \tag{1.25}$$

Substituting this back in Eq.(1.22) leads to

$$\dot{c}_m = -c_m\langle\psi_m|\dot{\psi}_m\rangle - \sum_{n\neq m} c_n \frac{\langle\psi_m|\dot{\hat{H}}|\psi_n\rangle}{E_n - E_m} e^{(i/\hbar)\int_0^t [E_n(t') - E_m(t')]dt'} \tag{1.26}$$

The second term may be dropped if we use the adiabatic approximation assuming that $\dot{\hat{H}}$ is sufficiently small. A solution to the equation after we drop the term is obtained by integration

$$c_m(t) = c_m(0)\text{exp}\left[i\left(i\int_0^t \langle\psi_m(t')|\partial_{t'}\psi_m(t')\rangle dt'\right)\right] = c_m(0)e^{i\gamma_m(t)} \tag{1.27}$$

Now let's assume the system have time dependence through a set of N parameters $\mathbf{R}(t) \equiv (R_1(t), R_2(t), ..., R_N(t))$, and the parameters change slowly over time so that the adiabatic approximation is valid then $\gamma_n(t)$ can be written as

$$\gamma_n(t) = i\int_0^t \langle\psi_n|\nabla_R\psi_n\rangle \cdot \frac{d\mathbf{R}}{dt'}dt' = i\int_{\mathbf{R_i}}^{\mathbf{R_f}} \langle\psi_n|\nabla_R\psi_n\rangle \cdot d\mathbf{R} \tag{1.28}$$

If the Hamiltonian completes a cycle after time-evolution say from time $t = 0$ to $t = T$ then

$\mathbf{R}(0) = \mathbf{R}(T)$ and

$$\gamma_n(t) = i \oint_{\mathcal{C}} \langle \psi_n | \nabla_R \psi_n \rangle \cdot d\mathbf{R} \tag{1.29}$$

where $\mathcal{C}$ is a closed path in parameter-space. Eq.(1.29) is called Berry phase. Defining a function called Berry connection which is a gauge-dependent quantity

$$\mathcal{A}_n(\mathbf{R}) = i\langle \psi_n | \nabla_R \psi_n \rangle \tag{1.30}$$

This let us write

$$\gamma_n(t) = i \oint_{C} \mathcal{A}_n(\mathbf{R}) \cdot d\mathbf{R} \tag{1.31}$$

Using Stokes' theorem one can write the Berry phase equation as

$$\gamma_n(t) = \int_S (\nabla_R \times \mathcal{A}_n) \cdot d\mathbf{S} \tag{1.32}$$

One may define

$$\mathcal{B}_n = \nabla_R \times \mathcal{A}_n = i\nabla_R \times \langle \psi_n | \nabla_R \psi_n \rangle \tag{1.33}$$

where $\mathcal{B}$ is called Berry curvature. The Chern number is defined as

$$C_n = \frac{1}{2\pi} \int d^2k \mathbf{e}_{k\perp} \cdot \mathcal{B} \tag{1.34}$$

where d^2k is Fermi surface, and $\mathbf{e}_{k\perp}$ is the unit vector normal to the Fermi surface. In the case of Weyl semimetal, the Chern number associated with right-handed chiral spinor is $C_n = +1$ and The Chern number associated with left-handed chiral spinor is $C_n = -1$. One can interpret the Weyl node as a monopole charge since the flux through the Fermi surface enclosing the Weyl node is nonzero . The Chern number can be considered as a topological charge of the Weyl node where the sign of the charge is determined by the chirality.

In metals, almost everything of consequence that's observable occurs on the Fermi surface. So, the corresponding momentum space invariant has to be defined on the Fermi surface in order

for metal to be topological. The flux of the Berry curvature through the two-dimensional Fermi surface of a three-dimensional metal is the only topological invariant that can be defined on the Fermi surface and leads to observable consequences.

Berry curvature is an analog to the magnetic field but it's defined in momentum space rather than real space. The Hamiltonian $H(\mathbf{k})$ in a crystal of noninteracting electrons is a matrix, whose elements are labelled by spin quantum numbers and atomic orbitals and which depends in $\mathbf{k}$ the crystal momentum as a parameter. The electronic structure is defined by the eigenvalues and eigenvectors of the equation

$$H(\mathbf{k})|u(\mathbf{k})\rangle = \epsilon(\mathbf{k})|u(\mathbf{k})\rangle \tag{1.35}$$

Let's consider an overlap between an eigenvector at point $\mathbf{k}$ and similar eigenvector taken at point in momentum space $\mathbf{k} + \delta\mathbf{k}$

$$\langle u(\mathbf{k})|u(\mathbf{k}+\delta\mathbf{k})\rangle \approx 1 + \delta\mathbf{k}\cdot\langle u(\mathbf{k})|\nabla_{\mathbf{k}}|u(\mathbf{k})\rangle \approx e^{i\mathcal{A}(\mathbf{k})\delta\mathbf{k}} \tag{1.36}$$

where $\mathcal{A}(\mathbf{k}) = -i\langle u(\mathbf{k})|\nabla_{\mathbf{k}}|u(\mathbf{k})\rangle$ is the Berry connection. Berry curvature as mentioned before is the curl of Berry connection

$$\mathcal{B}(\mathbf{k}) = \nabla_{\mathbf{k}} \times \mathcal{A}(\mathbf{k}) \tag{1.37}$$

Tha phase $\mathcal{A}(\mathbf{k})\delta\mathbf{k}$ can not be eliminated by a gauge transformation when the Berry curvature is nonzero and it leads to observable consequences

Suppose we have a nonzero flux of Berry curvature through a Fermi surface sheet. It's implied by Gauss' theorem that there must be a point of source or sink of the Berry curvature enclosed by this Fermi surface. Near this point, which is called Weyl node the Berry curvature takes a universal form up to trivial rescaling of the crystal momentum components

$$\mathcal{B} = \pm\frac{\mathbf{k}}{2k^3} \tag{1.38}$$

such that

$$C = \frac{1}{2\pi} \int \mathcal{B} \cdot d\mathbf{S} = \pm 1 \tag{1.39}$$

C is the above mentioned Chern number and the sign depends on whether the point a source or a sink.

A source or a sink point of the Berry curvature is obviously some sort of a singularity of the electronic structure. This singularity comes to be a point of degeneracy between two band. These degeneracy points are Weyl nodes. Fig(1.1) shows electronic structure of the simplest Weyl semimetal, with two nodes of opposite chirality, separated by a distance of $2k_0$ along the z-axis in momentum space. Similar to Berry curvature near the Weyl node take a universal form of the magnetic field of a point monopole, the Hamiltonian itself if expanded in the vicinity of Weyl node takes the following universal form as

$$H(\mathbf{k}) = \pm v_F \sigma \cdot \mathbf{k} \tag{1.40}$$

where the crystal momentum $\mathbf{k}$ is measured from the Weyl node. σ is Pauli matrices. The Hamiltonian is identical to the Hamiltonian proposed by Hermann Weyl in 1929 up to a replacement of v_F by the speed of light c.

Eq.(1.40) shows an essential property of topological metals which is their band eigenstate must be nondegenerate. This needs either broken spatial inversion when the crystal lacks a center of inversion or a broken time-reversal symmetry which happens in magnetic materials. Otherwise due to Kramers theorem all bands are doubly degenerate. Eq.(1.40) makes it clear that no other conditions are necessary for the existence of the Weyl band touching nodes in a 3D material. If either inversion symmetry or time-reversal symmetry are indeed broken the three components of the crystal momentum provide the necessary three real parameters needed to make two band eigenstate coincide in energy. So Weyl nodes happen generically in any 3D noncentrosymmetric or magnetic material.

A very interesting feature and key signature of Weyl semimetals is their surface states, which is

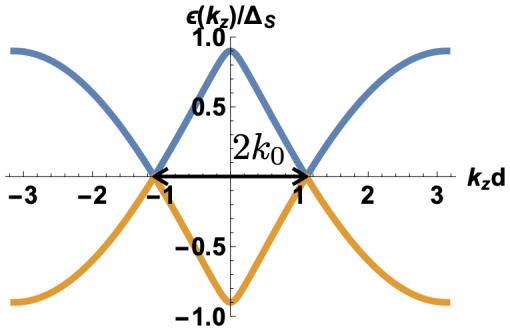

Figure 1.1: Electronic structure of the simplest Weyl semimetal, with two nodes of opposite chirality, separated by a distance of 2k0 along the z-axis in momentum space. Reprinted figure with permission of [8]

called Fermi arcs as shown in Fig(1.2). Usual materials have their Fermi surface a closed circle up to deformations on a two-dimensional surface. The Fermi surface in Weyl semimetals is different and only half of the usual Fermi circle stays in one surface, while the other half can be found on the opposed surface. Fermi arcs start and end at surface projections of the Weyl cones. Within the bulk band gap well-defined surface states can exist and typically are exponentially localized near the surface. When the bulk is gapless as in Weyl semimetals how can we define surface states. In this case we require to further assume translational invariance, thus we tag surface states by the crystal momenta within the 2D surface Brillouin zone. Then the regions of the surface Brillouin zone that are free of bulk states at the same energy are the only ones required. One can define surface states at same energy at all momenta except at the projection of the Weyl point onto the surface Brillouin zone, if we consider the idealized limit of a pair of Weyl nodes at the chemical potential ($E_F = 0$) at momenta $\pm \mathbf{k}_0^*$ in the surface Brillouin zone. Surface states can leak into the bulk even at $E_F = 0$ at those two points and are not well defined. The momentum region occupied by bulk states, if one consider other energies, grows as shown at the bottom of Fig(1.2) . Surface state that are impossible to realize in both strictly 2D and on the surface of any 3D insulator are allowed by the presence of these bulk states.

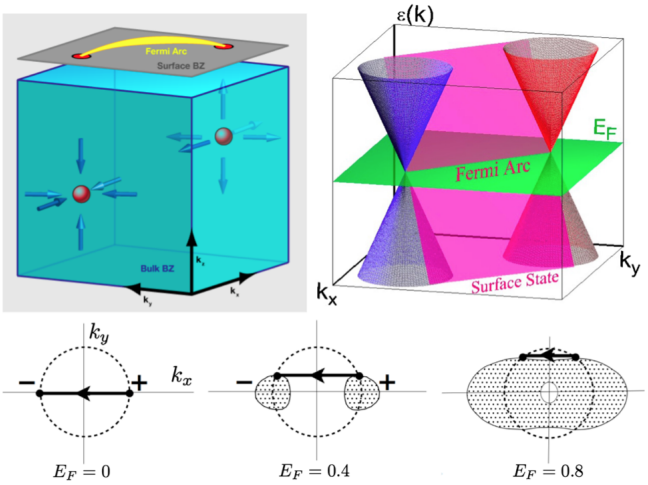

Figure 1.2: (Top left) Chern number, Weyl points, and Fermi arcs. (Top right) Connection of surface states to bulk Weyl points. (Bottom) Evolution of the Fermi arc with chemical potential in a particular microscopic model on raising the chemical potential from the nodal energy (E=0). Fermi arcs are tangent to the bulk Fermi surface projections and may persist even after they merge into a trivial bulk Fermi surface. Reprinted figure with permission of [9]

As mentioned above, either inversion symmetry or time reversal symmetry needs to be broken for Weyl semimetals. Two classes of Weyl semimetals were calculated and predicted theoretically. the first one is the broken time reversal symmetry candidates such as ferromagenetic hald-metal$HgCr_2Se_4$ and magenetic pyrochlories $A_2Ir_2O_7$. Also Co-based Heusler compounds were proposed as Weyl semimetals. The second one is broken inversion symmetry candidates. The tool that can directly observe the band structure of the material is angle-resolved photoemission spectroscopy (ARPES) and was used to get the band crossing and Weyl nodes in nonmagnetic Weyl semimetals. Multiple compounds were calculated by theorists in 2015 such as TaAs, TaP, NbAs and NbP Fig(1.3) (a) shows the structure of TaAs and shows that it doesn't have space inversion symmetry and (b) shows first-principles band structures calculation of TaAs. In the same year 2015 the Fermi arc and Weyl cones in TaAs as directly observed by ARPES indicating the realization of three-dimensional Weyl semimetal as shown in Fig(1.4). Later on more compounds were discovered theortically and observed experimentally.

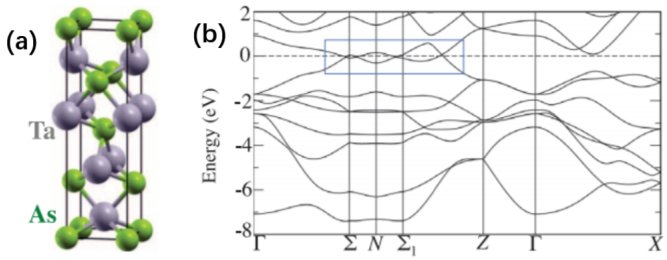

Figure 1.3: (a) Body-centered tetragonal structure of TaAs, shown as stacked Ta and As layers. The lattice of TaAs does not have space inversion symmetry.(b) First-principles band structure calculations of TaAs without spin-orbit coupling. The blue box highlights the locations where bulk bands touch in the BZ. Reprinted figure with permission of [14]

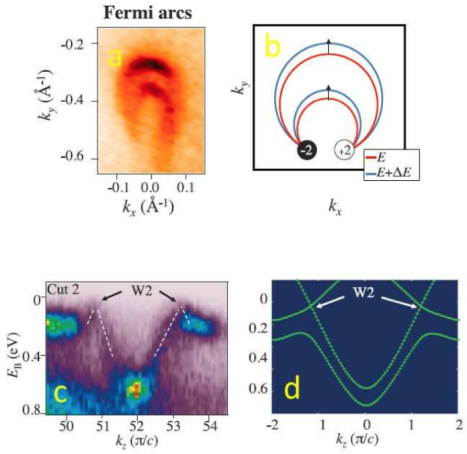

Figure 1.4: (a) High-resolution ARPES Fermi surface map of the crescent Fermi arcs.(b) A schematic showing the evolution of the Fermi arcs as a function of energy. (c)ARPES dispersion map along the cut 2 direction, showing that the W2 Weyl cone also disperses linearly along the out-of-plane direction.(d)First-principles calculated dispersion that corresponds to the cut 2 shown in (c).Reprinted figure with permission of [14]

Finally an introduction on Weyl semimetals cannot be complete without mentioning the types of Weyl semimetals. The previously known type is type I Weyl semimetal and the later discovered type is type II Weyl semimetal. To distinguish between the types we look at the Fermi surface. The Fermi surface of type I Weyl semimetal at Weyl point is point-like as shown in Fig (1.5). Weyl fermions are emerging at boundary between electron and hole pockets in type II Weyl semimetal. the Weyl cone for type II has a tilted shape since the Weyl point is different even though it is still linearly dispersive.

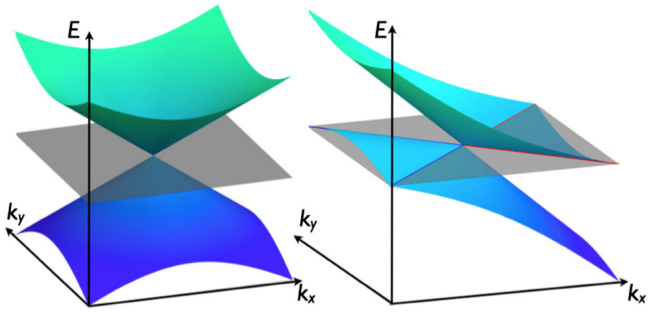

Figure 1.5: (Left) Conventional type I point with point-like Fermi surface. (Right) Type II Weyl point is the touching point between electron and hole pockets. Red and blue (highlighted) isoenergy contours denote the Fermi surface coming from electron and hole pockets with chemical potential tuned to the touching point. Reprinted figure with permission of [9]

2. FOUR-WAVE MIXING IN WEYL SEMIMETALS[1]

2.1 Introduction

Weyl semimetals (WSMs) are fascinating materials with nontrivial topology of both bulk and surface electron states [8, 9, 12, 13, 14, 15, 16, 17, 18]. Although most of the research on WSMs has been focused on their electronic structure and transport, a number of recent studies have suggested that WSMs should also have highly unusual optical properties. For example, Kerr and Faraday rotations were predicted [19]. The evolution of the interband response within a model Hamiltonian which contains Dirac, Weyl, and gapped semimetal phases is studied [20]. The plasmon modes which have damping rates more than an order of magnitude smaller compared to the energy were predicted [21]. The theory of topological Fermi arc plasmons was developed in [22]. Negative refraction was shown theoretically that it can occur in WSM and the refractive index is negative at specific frequency range close to the plasmon frequency [23]. The electronic band-structure calculations can effectively explain the optical conductivity spectra of typical WSMs without electron correlation [24]. The existence of nonreciprocal waveguides modes in ferromagnetic WSM films in the Voigt configuration without an external magnetic field is predicted [25]. It's shown that the component of the permittivity tensor normal to the interfaces can achieve an ϵ-near-zero (ENZ) response depending on the Weyl cone tilt, chemical potential, and electromagnetic wave frequency [26]. A dissipationless second-order anomalous node conductivity for WSMs belonging to the TaAs family is predicted [27]. It's shown how information about electronic structure of Weyl semimetals, such as the position and separation of Weyl nodes, Fermi energy, and Fermi arc surface states, can be unambiguously extracted from measurements of the dispersion, transmission, reflection, and polarization of electromagnetic waves[28]. By calculating the frequency-, polarization-, and temperature-dependent complex dielectric functions using a microscopic picture of the relevant electron-electron and electron-phonon interactions in each material, a concrete

[1]Reprinted with permission from "Four-wave mixing in Weyl semimetals" by Sultan Almutairi, Qianfan Chen, Mikhail Tokman, and Alexey Belyanin, Phys. Rev. B 101, 235156, Copyright 2020 by The American Physical Society

link between Weyl physics, scattering processes, and experimentally relevant optical quantities is established [29]. Information about Weyl node position and separation, the value of the Fermi momentum, and the matrix elements of the optical transitions involving both bulk and surface electron states is provided by Strong anisotropy, gyrotropy, and the optical Hall effect for surface polaritons launched by a nanotip [30].

Due to the presence of one or more pairs of separated Weyl nodes, the electron bandstructure of WSMs is highly anisotropic and (in the case of time-reversal symmetry-breaking WSMs) gyrotropic. As a result, even in the weak-field linear regime the optical conductivity tensor is quite complicated and generally cannot be expressed analytically even within the simple microscopic model of a two-band WSM Hamiltonian with two separated Weyl nodes ([32, 33]); see e.g. [28, 30] where bulk and surface conductivity tensors were derived and the properties of bulk and surface electromagnetic eigenmodes were described. Fortunately, one expects the strongest nonlinear optical response in the high-doping, long-wavelength limit $\hbar\omega \ll E_F, \hbar v_F b$, where E_F is the Fermi energy and $2\hbar b$ is the Weyl point separation in momentum space [28]. In this limit the electron bandstructure takes a simple universal form of 3D cones for both Dirac and Type-I Weyl semimetals. As a result, one can obtain analytic, although a bit cumbersome, expressions for the nonlinear conductivity of any order.

There are several reasons why the power of the nonlinear four-wave mixing (FWM) efficiency from WSMs should be high in the long-wavelength limit. First, the dispersion of massless Weyl fermions is, of course, very far from parabolic, which ensures strong nonlinearity of intraband electron oscil- lations in an external optical field. This is to be contrasted with electrons near the conduction band minimum of conventional semiconductors that are only weakly nonparabolic: see, for example, Refs. [34, 35, 36] where the third-order intraband non- linear response due to band nonparabolicity has been observed and explained.

Second, the magnitude of the dipole matrix element of the optical transitions between two states $|n\rangle$ and $|m\rangle$ with eigenenergies ϵ_n and ϵ_m is $\vec{\mu}_{mn} = e \cdot \langle m|\mathbf{r}|n\rangle = \frac{i\hbar e}{\epsilon_n - \epsilon_m}\langle m|\hat{\mathbf{v}}|n\rangle$. For electron systems with continuous energy spectra, the main contribution to the optical response at

frequency ω comes from energy states separated by $\epsilon_n - \epsilon_m = \hbar\omega$. Furthermore, for massless fermions, the magnitude of the velocity is constant: $\hat{\mathbf{v}} = v_F\hat{\vec{\sigma}}$, i.e., $|\mathbf{v}| = v_F$, where v_F is the Fermi velocity. Therefore, the magnitude of the dipole moment scales as $\mu \sim ev_F/\omega$. This is true for both intraband and interband transitions. Note the linear scaling with wavelengthλ, $\mu \propto \lambda$for Weyl fermions as compared to the usual $\mu \propto \sqrt{\lambda}$ scaling for massive electrons with parabolic dispersion. As a result, the nonlinear nth order conductivity grows rapidly,$|\sigma^{(n)}| \propto \mu^{n+1}$, with increasing wavelength. Taking into account the density of states, one can immediately predict the scaling $|\sigma^{(3)}| \propto \dfrac{e^4 v_F}{(\hbar\omega)^3}$ which is confirmed below. The resulting magnitude of $|\chi^{(3)}|$ is many orders of magnitude higher than in conventional nonlinear materials.

The third reason is that at low frequencies $\hbar\omega \ll 2E_F$, the interband absorption is eliminated by Pauli blocking. Finally, the electric field of the nonlinear signal is enhanced in the vicinity of bulk plasma resonance due to the boundary conditions at the interface. The latter effect is similar to the observed enhancement of Kerr index modulation and third- harmonic generation in so-called epsilon-near-zero materials; see, e.g., Refs. [37, 38]. An exceptionally high value of $|\chi^{(3)}|$ in combination with field enhancement at plasma resonance lead to a surprisingly high efficiency of the nonlinear generation, of the order of several mW per W^3 of incident pump power.

The third order conductivity has been calculated by [39] in the hydrodynamic limit and for frequencies lower than the scattering rate $1/\tau$. Here we are interested in the frequencies higher than the scattering rate, but still low enough to limit the response to the vicinity of the Weyl points, as argued above. There is some controversy surrounding this low-frequency kinetic limit of the third-order response. In [40] the third-order conductivity in the terahertz spectral range was calculated for degenerate FWM ($\omega + \omega - \omega$) and third-harmonic generation processes. However, in a very recent paper [41] the third-order conductivity was found to be zero in the low-frequency limit and zero result was rationalized by symmetry arguments. While the inversion symmetry prohibits the nonzero *second-order* response in electric-dipole approximation, we don't see any symmetry arguments that would require the third-order response of WSMs to be zero, even assuming perfectly isotropic conical dispersion near every Weyl point. And indeed, we present a very general kinetic

equation-based derivation of the third-order conductivity to show that it remains finite and in fact quite large in magnitude at low frequencies.

In Sec. 2.2, we derive the general expression for the third-order nonlinear conductivity by using the kinetic equation formalism for frequencies higher than the phenomenological relaxation rate. We then proceed in Sec. 2.3 to calculate the four-wave mixing (FWM) signal power transmitted through a WSM slab or propagating away from the surface of the material opposite to the direction of incident pump beams. as a function of relevant parameters such as frequency and doping level. The Appendix contains the derivation of the third-order susceptibility.

2.2 Third-Order Nonlinear Optical Conductivity

We consider the optical response of a doped WSM at frequencies $1/\tau < \hbar\omega < 2E_F$ that are low enough so that the electron excitations in the vicinity of each Weyl point satisfy the linear dispersion:

$$E_s = s\mathbf{v}\cdot\mathbf{p}, \tag{2.1}$$

where $s = \pm 1$ is for the conduction and valence bands, respectively. We assume for simplicity that the velocity has the same magnitude in every direction, i.e. the cone is isotropic. Anisotropic cones can be easily incorporated into the analytic theory below, but they will make the expressions more cumbersome without changing the nonlinear response qualitatively. We will assume for definiteness that the Fermi level is in the conduction band. Thus we have

$$\mathbf{v} = \frac{\partial E_+}{\partial \mathbf{p}} = v_F\mathbf{n}, \tag{2.2}$$

where E_+ is the electron energy in the conduction band, $p = \sqrt{p_x^2 + p_y^2 + p_z^2}$ is the magnitude of electron momentum, v_F is the Fermi velocity, and $\mathbf{n} = \frac{\mathbf{p}}{p} = (\sin\theta\cos\phi, \sin\theta\sin\phi, \cos\theta)$ is the unit vector in the direction of the electron velocity.For $\hbar\omega < 2E_F$ and in the limit of strong Fermi degeneracy, intraband transitions make the dominant contribution. When only the intraband transitions are included, the fully quantum approach based on the von Neumann equation for the density matrix gives the same result as the semiclassical kinetic equation approach. For massless

2D Dirac fermions, this was checked explicitly in [42]. The kinetic equation with a phenomenological collision term has a standard form:

$$\frac{\partial f}{\partial t} + v_F(\mathbf{n}\cdot\nabla)f - [e\mathbf{E} + \frac{v_F}{c}(\mathbf{n}\times\mathbf{B})]\cdot\frac{\partial f}{\partial \mathbf{p}} = \gamma[F(p) - f], \tag{2.3}$$

where $\mathbf{E}$ and $\mathbf{B}$ are external electric and magnetic fields, respectively, e is the electron charge, γ is the electron relaxation rate, $F(p)$ is an unperturbed (zeroth-order) distribution function, which is chosen as the equilibrium Fermi-Dirac distribution, and f is the non-equilibrium distribution function in the presence of external fields.We are interested in the electric-dipole optical response, so we will neglect the magnetic-field-dependent terms and the terms with spatial gradients in Eq. (2.3). The latter would lead to corrections that scale as powers of the small parameter $v_F/(L\omega)$, where L is a characteristic scale of the optical field nonuniformity in the material [42, 43]. In a transparent medium, L would be equal to the wavelength of radiation.

The current density can be then calculated as

$$\mathbf{j}(\mathbf{r},t) = -e\int \mathbf{v} f(\mathbf{r},\mathbf{p},t)\, d^3p. \tag{2.4}$$

We are interested in the electric-dipole optical response, so the magnetic field term can be neglected. We also assume that the electric field has the form

$$\mathbf{E}(\mathbf{r},t) = \sum_n \mathbf{E}_n(\mathbf{r},\omega_n)e^{-i\omega_n t} = \sum_n \mathbf{A}_n e^{ik_n x - i\omega_n t}, \tag{2.5}$$

and make an ansatz for the non-equilibrium distribution function:

$$f = \sum_m \xi_m e^{iq_m x - i\omega_m t}, \tag{2.6}$$

where we have set $\xi_0 = F(p)$, $E_0 = 0$, $\omega_0 = 0$. Because both the electric field and the non-equilibrium distribution function are real, i.e. $\mathbf{E}(\mathbf{r},t) = \mathbf{E}^*(\mathbf{r},t)$ and $f = f^*$, we obtain $E_{-n} = E_n^*$,

$\xi_{-n} = \xi_n^*$, $\omega_{-n} = -\omega_n$.,$q_{-n} = -q_n$

In the Appendix, we perturbatively solve the Boltzmann equation up to the third order under the above conditions. In particular, we show that an optical response at any order for an arbitrary non-degenerate multi-wave mixing can be calculated by the repetitive applying of the following operator to the equilibrium distribution function:

$$\begin{aligned} G^{n,m}(p,\phi,\theta) &\equiv g_1^{n,m}(\phi,\theta)\frac{\partial}{\partial p} + g_2^{n,m}(\phi,\theta)\frac{\partial}{p\partial\phi} \\ &\quad + g_3^{n,m}(\phi,\theta)\frac{\partial}{p\partial\theta}, \end{aligned} \tag{2.7}$$

where p, ϕ, θ are spherical coordinates in momentum space and

$$g_1^{n,m}(\phi,\theta) \equiv e\frac{E_{m,x}\cos\phi\sin\theta + E_{m,y}\sin\phi\sin\theta + E_{m,z}\cos\theta}{-i\omega_n + \gamma}, \tag{2.8}$$

$$g_2^{n,m}(\phi,\theta) \equiv e\frac{E_{m,y}\cos\phi - E_{m,x}\sin\phi}{\sin\theta(-i\omega_n + \gamma)} \tag{2.9}$$

$$\begin{aligned} g_3^{n,m}(\phi,\theta) &\equiv (E_{m,x}\cos\phi\cos\theta + E_{m,y}\sin\phi\cos\theta - E_{m,z}\sin\theta) \\ &\quad \times\frac{e}{(-i\omega_n + \gamma)}. \end{aligned} \tag{2.10}$$

For example, the first-order approximation describing the linear optical response is

$$\xi_n^{(1)} = G^{n,n}\xi_0 = g_1^{(n,n)}\frac{\partial F}{\partial p}. \tag{2.11}$$

Substituting this into Eq. (2.4) and using $\int_0^\infty \frac{\partial F(p)}{\partial p}p^2dp = -p_F^2$ in the strong degeneracy/low temperature limit, one can get

$$\sigma^{(1)}(\omega) = \frac{e^2 v_F p_F^2 g_s g_w}{6\pi^2\hbar^3(\gamma - i\omega)}, \tag{2.12}$$

where g_s and g_w are the degeneracy factors associated with spin and the number of Weyl nodes respectively.

The second-order approximation of the non-equilibrium distribution function is $\xi_l^{(2)}$,

$$\xi_l^{(2)} = \sum_{m,k} G^{l,m}\xi_k^{(1)} = \sum_{m,k} G^{l,m}G^{k,k}\xi_0 \tag{2.13}$$

for all possible ω_m and ω_k satisfying the relation $\omega_l = \omega_m + \omega_k$. Similarly, the third-order response is described by

$$\xi_i^{(3)} = \sum_{j,m,k} G^{i,j}\xi_l^{(2)} = \sum_{j,m,k} G^{i,j}G^{l,m}G^{k,k}\xi_0 \tag{2.14}$$

for all possible ω_j, ω_m and ω_k satisfying the relation $\omega_i = \omega_j + \omega_m + \omega_k$. The nonlinear current $\mathbf{j}(\omega_n = \omega_1 + \omega_2 + \omega_3)$ is then given by

$$\begin{aligned}
\begin{pmatrix} j_x \\ j_y \\ j_z \end{pmatrix} &= -ev_F \int_0^{\infty}\int_0^{2\pi}\int_0^{\pi} \xi_n^{(3)} \begin{pmatrix} \cos\phi\sin\theta \\ \sin\phi\sin\theta \\ \cos\theta \end{pmatrix} p^2 \sin\theta dp d\theta d\varphi \\
&= \sigma_{ijkl}E_1^j E_2^k E_3^l
\end{aligned} \tag{2.15}$$

In the strong degeneracy/low temperature limit the integral can be evaluated analytically; see the Appendix. The resulting third-order nonlinear optical conductivity tensor has the form

$$\begin{aligned}
\sigma_{ijkl} &= \frac{e^4 v_F g_s g_w \Delta_{ijkl}}{90\pi^2\hbar^3(\gamma - i\omega_1)} \frac{1}{[\gamma - i(\omega_1+\omega_2)]\,[\gamma - i(\omega_1+\omega_2+\omega_3)]} \\
&+ \quad \text{all permutations of } \omega_1, \omega_2, \omega_3,
\end{aligned} \tag{2.16}$$

where $\Delta_{ijkl} \equiv \delta_{ij}\delta_{kl} + \delta_{ik}\delta_{jl} + \delta_{il}\delta_{jk}$. Here δ_{ij} is the Kronecker delta.

In the particular case of the third harmonic generation $\omega_1 = \omega_2 = \omega_3 = \omega$. Then the nonlinear current at $\omega_n = 3\omega$ is

$$j_k^{(3)}(3\omega) = \frac{e^4 v_F g_s g_w (E_{1,x}^2 + E_{1,y}^2 + E_{1,z}^2)}{5\pi^2\hbar^3(\gamma - i3\omega)(\gamma - i2\omega)(\gamma - i\omega)} E_{1,k}, \tag{2.17}$$

where $k = (x, y, z)$. This is consistent with the result for $\sigma_3^{intra}(3\omega)$ in [40] when $E_{1,x,y,z} = E_0$.

In another special case of partially degenerate FWM we consider the nonlinear current at frequency $\omega_s = 2\omega_1 - \omega_2$. For simplicity, we assume that the electric field is along the z-axis; then the z-component of the nonlinear current is

$$j_z^{(3)}(\omega_s) = \frac{e^4 v_F g_s g_w E_{1,z}^2 E_{2,z}^*}{15\pi^2\hbar^3(-i\omega_s+\gamma)}\left[\frac{\frac{1}{i\omega_2+\gamma}+\frac{1}{-i\omega_1+\gamma}}{(-i(\omega_1-\omega_2)+\gamma)} + \frac{1}{(-i2\omega_1+\gamma)(-i\omega_1+\gamma)}\right]. \tag{2.18}$$

Note the resonance at $\omega_1 = \omega_2$. The absolute value of the third-order susceptibility $\chi^{(3)} = \frac{i\sigma^{(3)}}{\omega_s}$ which follows from Eq. (2.18) is plotted in Fig.(2.1) as a function of detuning $\delta\omega = \omega_2 - \omega_1$ for several values of ω_1. The magnitudes of $\chi^{(3)}$ are many orders of magnitude higher as compared to typical values in the conventional nonlinear crystals [1]. However, strong optical absorption in WSMs limits the nonlinear signal power, as we show in the next section.

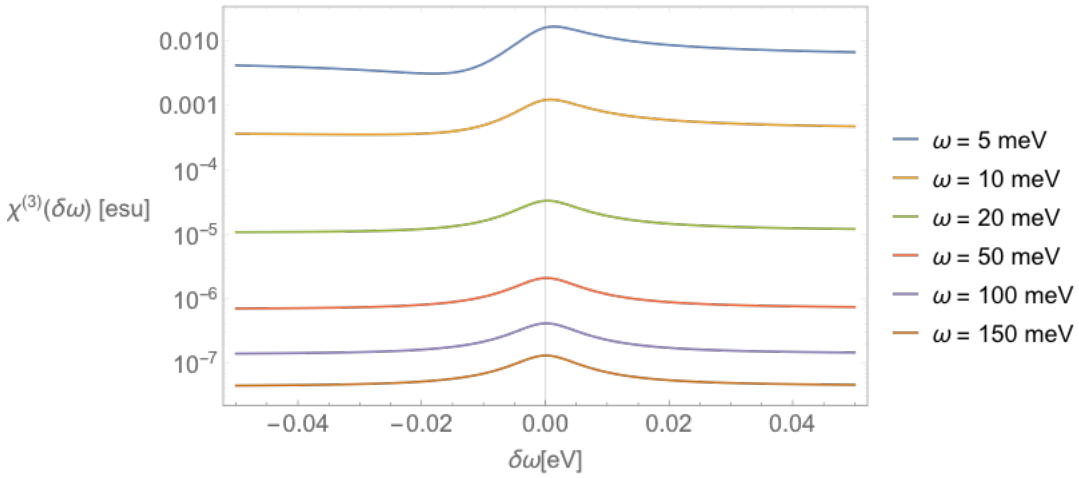

Figure 2.1: The absolute value of $\chi^{(3)}$ as a function of detuning $\delta\omega = \omega_2 - \omega_1$ for several values of ω_1. Other parameters are $\hbar\gamma = 5$ meV, $v_F = 10^8$ cm/s, $g_s = 2$, $g_w = 4$. Reprinted figure with permission of [44]

2.3 Intensity and Power of the Nonlinear FWM Signal

As the simplest problem relevant to the experiment, we consider two monochromatic pump fields at frequencies ω_1 and ω_2 normally incident at the WSM layer from the air. The case of an oblique incidence can be easily solved in the same way, but we will try to keep the expressions less cumbersome. The nonlinear FWM signal at frequency $\omega_s = 2\omega_1 - \omega_2$ is generated by the nonlinear current inside the WSM material. It can be observed both in the transmission geometry, i.e. propagating through the WSM layer, or in the reflection geometry where it propagates away from the WSM surface into the air, opposite to the direction of the incident pump beam. Although there is no incident nonlinear signal, the presence of the "reflected" wave is mandated by the boundary conditions, since the nonlinear current exists only on one side of the air-WSM interface.

First, it is instructive to find the linear dispersion and absorption of EM waves propagating in the bulk WSM. Since the material is isotropic within our model, the normal modes are transverse waves with the wave vector magnitude $k = \frac{n(\omega)\omega}{c}$. Here $n(\omega) = \sqrt{\epsilon(\omega)}$ and $\epsilon(\omega) = \epsilon_b + \frac{4\pi i\sigma^{(1)}}{\omega}$, where ϵ_b is the background dielectric permittivity due to off-resonant transitions to remote bands and $\sigma^{(1)}$ is the linear response of Weyl fermions given by Eq. (2.12). The absorption length can be obtained as $L_{ab}(\omega) = \dfrac{c}{\omega \mathrm{Im}\,[n]}$.

Fig.(2.2a), and Fig.(2.2b) show real and imaginary parts of the linear refractive index as a function of frequency at different Fermi energies. At low frequencies the linear response is dominated by the plasmonic response of Weyl fermions. The plasmonic resonance $\mathrm{Re}[\epsilon(\omega)] = 0$ is clearly visible in the refractive index spectra. Below the plasmonic resonance the absorption length drops to the values shorter than the wavelength. Note that the plots cannot be applied to the interband transition region $\hbar\omega > 2E_F$.

Next, we calculate the intensity and power of the nonlinear signal. Assume that the interface between the WSM and the air is in the (x, y) plane and the WSM is at $z > 0$.As shown in Fig .(2.3) EM fields in the air above the WSM consist of incident and reflected pump waves, $E_{i1,2}e^{i(\omega_{1,2}/c)z}$ and $E_{r1,2}e^{-i(\omega_{1,2}/c)z}$, and the nonlinear signal wave propagating away from the interface: $E_a = E_a^{(-)}e^{-ik_0 z}$, where $k_0 = \omega_s/c$. Here we assume that all fields are linearly polarized in the same

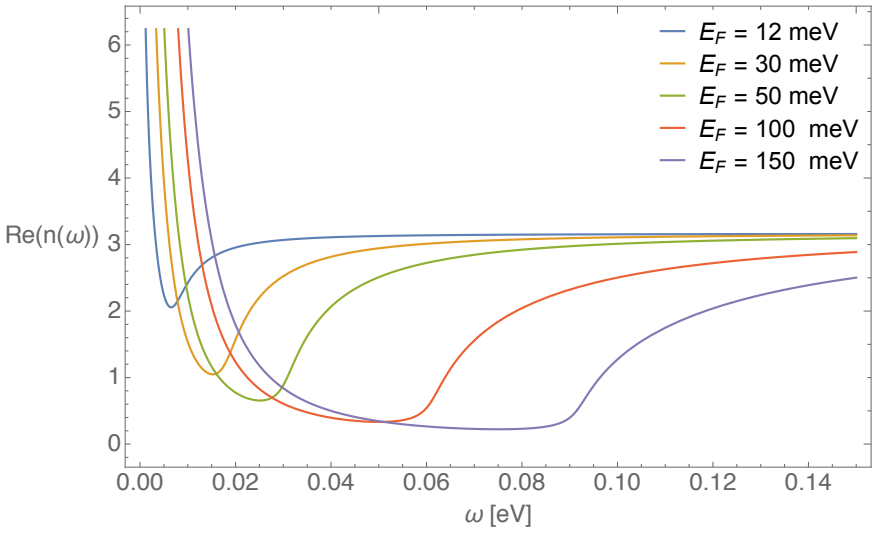

(a)

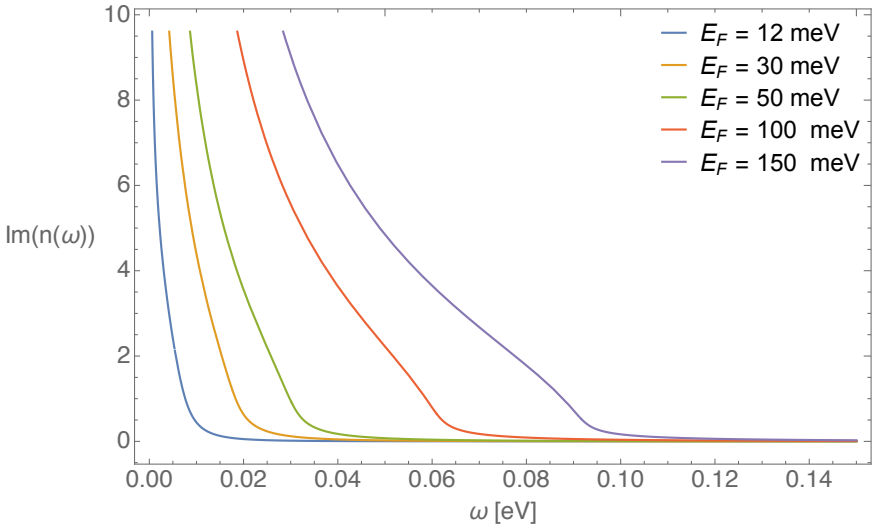

(b)

Figure 2.2: (a)Real part of the linear refractive index as a function of frequency at different Fermi energies for $\epsilon_b = 10$, $\hbar\gamma = 5$ meV, $v_F = 10^8$ cm/s, $g_s = 2$, $g_w = 4$. (b)Imaginary part of the linear refractive index as a function of frequency at different Fermi energies for $\epsilon_b = 10$, $\hbar\gamma = 5$ meV, $v_F = 10^8$ cm/s, $g_s = 2$, $g_w = 4$. Reprinted figure with permission of [44]

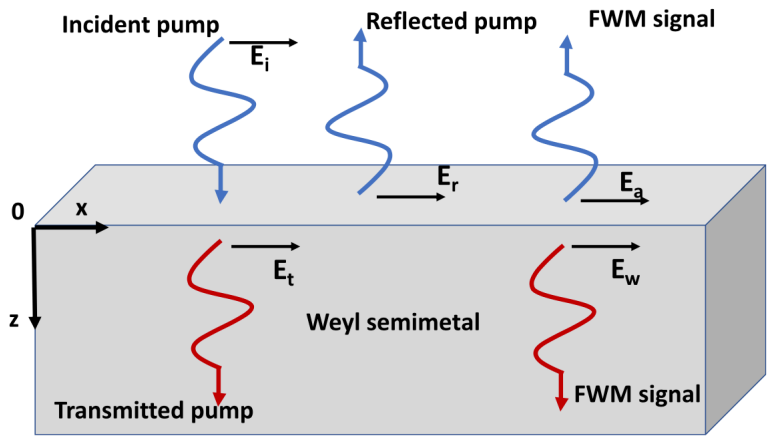

Figure 2.3: Sketch of the simplest experimental geometry. The third- order nonlinear current generated in bulk WSM by incident pump beams gives rise to the FWM signals propagating both into and out of the material. Reprinted figure with permission of [44]

direction and drop the polarization vectors.

The EM fields in the WSM consist of transmitted pump waves $t_{1,2}E_{i1,2}e^{ik_{1,2}z}$ where $t_{1,2}$ are Fresnel transmission coefficients for the field at frequencies $\omega_{1,2}$, and the copropagating nonlinear signal. The nonlinear correction to the refractive index for the pump waves in the WSM is not important because they interact with the signal wave over a short distance comparable or smaller than the wavelength, as we will see below. The monochromatic electric field of the nonlinear signal at frequency ω_s satisfies Maxwell's wave equation with the nonlinear polarization$P^{(3)}(\omega_s)$ as the source term and appropriate boundary conditions for electric and magnetic fields at z = 0:

$$\nabla^2 E_w(\omega_s) + \epsilon(\omega_s)k_0^2 E_w(\omega_s) = \frac{-4\pi\omega_s^2}{c^2}P^{(3)}(\omega_s), \tag{2.19}$$

After expressing the nonlinear polarization through the third- order susceptibility and the pump fields in the material, the right-hand side of Eq. (2.19) can be written as

$$\frac{d^2E_w}{dz^2} + \epsilon(\omega_s)k_0^2E_w = Ae^{ikz}, \tag{2.20}$$

where $k \equiv 2k_1 - k_2$ and

$$A = -\frac{4\pi\omega_s^2}{c^2}\chi^{(3)}t_1^2t_2^*E_{i1}^2E_{i2}^*. \tag{2.21}$$

Note that the dielectric function $\epsilon(\omega)$ is complex at all frequencies and therefore all relevant wavenumbers are complex: $k_{1,2} = (\omega_{1,2}/c)n_{1,2}$, $k_s = k_0n_s$, where $n_{1,2} = \sqrt{\epsilon(\omega_{1,2})}$, $n_s = \sqrt{\epsilon(\omega_s)}$, and all imaginary parts $\mathrm{Im}[n_{1,2,s}]$ are greater than zero.

The solution to Eq. (2.20) can be written as a sum of the general solution to the homogeneous part and a particular solution to the inhomogeneous equation:

$$E_w = E_w^{(+)}e^{ik_sz} + \frac{A}{k_s^2 - k^2}e^{ikz}, \tag{2.22}$$

where we dropped the $E_w^{(-)}e^{-ik_sz}$ term.

The continuity of the tangential electric and magnetic fields at the interface $z = 0$ give $E_a = E_w$ and $\frac{dE_a}{dz} = \frac{dE_w}{dz}$, or

$$\begin{aligned} E_a^{(-)} &= E_w^{(+)} + \frac{A}{k_s^2 - k^2} \\ -k_0E_a^{(-)} &= k_sE_w^{(+)} + k\frac{A}{k_s^2 - k^2}. \end{aligned} \tag{2.23}$$

This leads to the following expressions for the nonlinear signal fields propagating from the interface into the air and into the WSM:

$$\begin{aligned} E_a &= \frac{1}{k_s + k_0}\frac{A}{k_s + k}e^{-ik_0z}, \\ E_w &= \frac{A}{k_s^2 - k^2}\left(e^{ikz} - \frac{k_0 + k}{k_0 + k_s}e^{ik_sz}\right), \end{aligned} \tag{2.24}$$

where as a reminder $k = 2k_1 - k_2$. These expressions can be used to calculate the nonlinear signal power in both transmission and reflection geometry. For the transmission geometry, when

the pumps and the nonlinear signal co-propagate through a WSM film, it makes no sense to take the films thicker than the absorption length of the field. The maximum power is reached when the film thickness is of the order of the absorption length $L_{abs} = 1/\mathrm{Im}[k_s]$.

In the absence of any dissipation (i.e. when all wavenumbers are real) and for exact phase matching $k_s \to k$, the signal field propagating into the WSM grows linearly with z, as expected:

$$E_w = A\frac{e^{ik_s z}}{2k_s}\left(\frac{1}{k_0+k_s} - iz\right);\ E_a = \frac{A}{2k_s(k_s+k_0)}e^{-ik_0 z}. \tag{2.25}$$

Of course, for realistic fields of finite duration, the region of linear growth of the field is limited by the pulse duration. Moreover, field dissipation is always important because of a fast electron scattering rate γ expected in real materials and especially in the region around plasma resonance.

Figure (2.4) shows the power of the nonlinear signal in the reflection geometry, in W per W^3 of incident pump power, for degenerate FWM with $\omega_1 = \omega_2$ and assuming that all beams are focused into an area of vacuum wavelength squared, i.e. $P_a = \frac{c}{2\pi}|E_a|^2\left(\frac{2\pi}{k_0}\right)^2$ and similarly for the pump. All other parameters are the same as in Fig.(2.2).

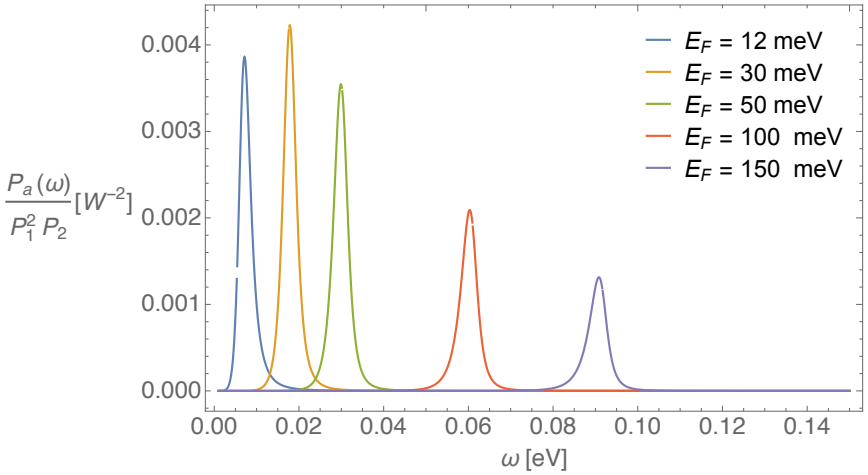

Figure 2.4: The nonlinear signal power in reflection geometry, i.e. when the signal propagates away from the interface into the air, as a function of frequency and for several values of the Fermi energy. Reprinted figure with permission of [44]

The sharp peaks in the spectrum are entirely due to a strong dependence of the signal field intensity from the refractive index of the WSM:

$$|E_a|^2 = \frac{256\pi^2|\chi^{(3)}|^2}{|n_s|^2|n_s+1|^8}|E_i|^6. \tag{2.26}$$

Indeed, the absolute value of the refractive index has a sharp minimum in the vicinity of plasma resonance, see Fig.(2.5), that are manifested in the power spectra. Note a simple "universal " character of the expression Eq. (2.26) for the nonlinear signal, especially given the fact that the value of $\chi^{(3)}$ in this expression does not depend on the Fermi energy. The Fermi energy dependence in Eq. (2.26) which is shown in Fig.(2.4) enters entirely through the refractive index n_s.

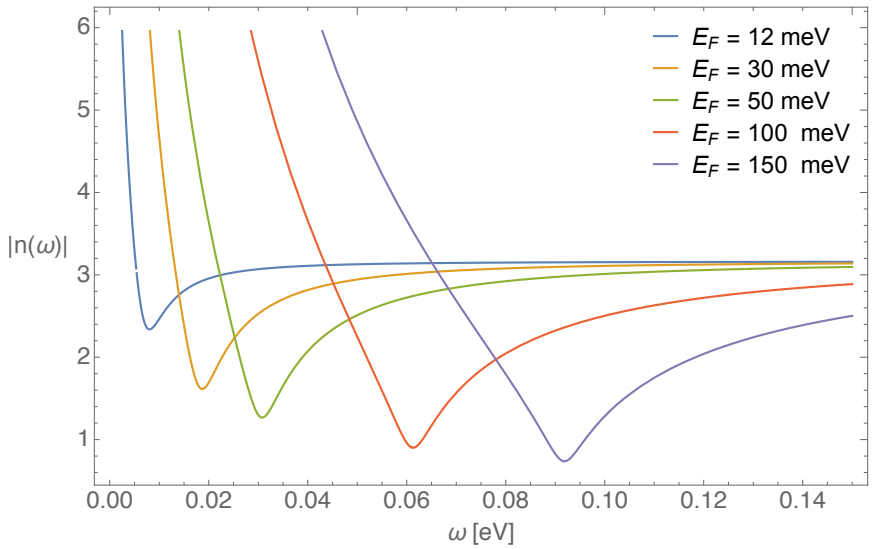

Figure 2.5: Absolute value of the linear refractive index as a function of frequency at different Fermi energies for $\epsilon_b = 10$, $\hbar\gamma = 5$ meV, $v_F = 10^8$ cm/s, $g_s = 2$, $g_w = 4$. Reprinted figure with permission of [44]

The efficiency of the FWM process is quite high, a few mW per W^{3}3 of incident pump power, especially in view of the fact that the reflected nonlinear signal is generated in the subwavelength skin layer below the air/WSM interface. It originates from the high magnitude of $|\chi^{(3)}|$ and strong

refractive index dependence mandated by the boundary conditions. The sharp increase in the FWM signal near plasma resonance is conceptually similar to the predicted and observed enhancement of the third-order nonlinear effects for intense laser field propagating in epsilon-near-zero materials; see, e.g., Refs. [37, 38] or the recent reviews [45, 46] and references therein.

With detuning from resonance $\delta\omega = \omega_2 - \omega_1 = 0$, the FWM power will decrease following$|\chi^{(3)}| \propto 1/(\delta\omega)^2$ as one can see from Eq. (2.18) and Fig. (2.1).

The field intensity of the transmitted nonlinear signal in the degenerate FWM process at the distance z into the sample is given by

$$|E_w|^2 = \frac{256\pi^2|\chi^{(3)}|^2|E_i|^6}{|n_s|^2|n_s+1|^6}\left|\frac{1}{1+n_s} - ik_0 z\right|^2 e^{-2k_0 \mathrm{Im}[n_s]z}. \tag{2.27}$$

The corresponding power after propagating a distance equal to the absorption length $L_{ab} = 1/\mathrm{Im}[k_s]$ into the sample is plotted in Fig.(2.6) as a function of frequency for different Fermi energies. Here we again assumed that the pump beam was focused into the area of $(2\pi/k_0)^2$.

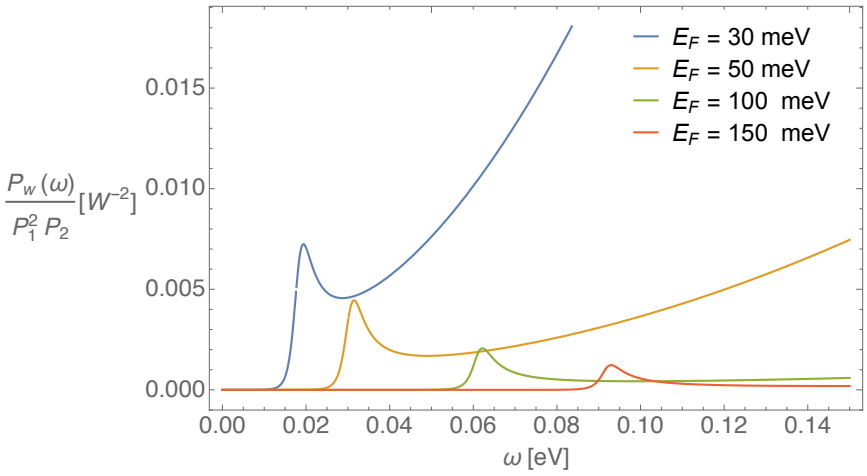

Figure 2.6: The nonlinear signal power after propagating a distance equal to one absorption length $L_{ab} = 1/\mathrm{Im}[k_s]$ into the sample, as a function of frequency and for several values of the Fermi energy. Reprinted figure with permission of [44]

The characteristic feature of each spectrum is a sharp peak just above plasma resonance, when the refractive index $n_s(\omega)$ is still close to its minimum value, followed by a gradual increase. This increase is entirely due to the absorption length increasing with frequency, as shown in Fig.(2.7). Note however that the plots in Figs.(2.6) and 2.7 cannot be extended beyond $\omega = 2E_F$ where the interband transitions become important.

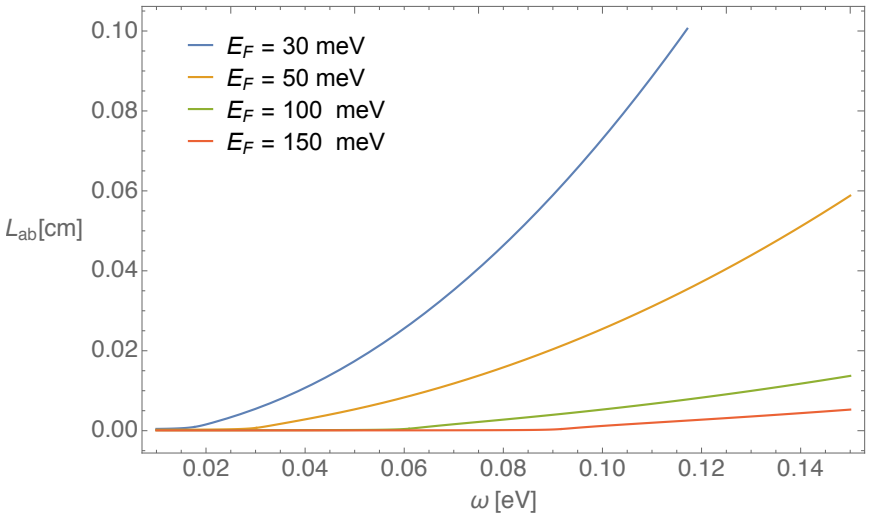

Figure 2.7: Absorption length $L_{ab} = 1/\text{Im}[k_s]$ as a function of frequency at different Fermi energies for $\epsilon_b = 10$, $\hbar\gamma = 5$ meV, $v_F = 10^8$ cm/s, $g_s = 2$, $g_w = 4$. Reprinted figure with permission of [44]

Therefore, for a sample with a given electron density one can get similar levels of the transmitted nonlinear signal power when using a very thin film at frequencies near the plasma resonance enhancement and when using thicker films at higher frequencies near the interband transitions cutoff. This is illustrated in Fig.(2.8) which shows the nonlinear signal power as a function of distance into the sample at two different frequencies and the same Fermi level.

Various strategies can be employed to extract the transmit- ted nonlinear signal from the sample on the bottom side of the WSM film: an index-matching substrate, tailoring the layer thicknesses to form a Fabry-Perot cavity or a coupled cavity, etc. We won't go into these technical details here.

Moreover, since the magnitudes of the signal power in transmission and reflection geometries are similar (compare Figs. 2.4 and 2.8), in many cases it is more convenient to use the reflected (backward-propagating) FWM signal |Ea|2 which is formed in the subwavelength layer of the order of skin depth at the surface. Then the details of the substrate and actual sample thickness don't matter, as long as this thickness is much larger than the skin depth. Since the electric field decays exponentially into the sample over the scale of the skin depth, the structure of the sample at several or more skin depths below the surface can't affect the signal.

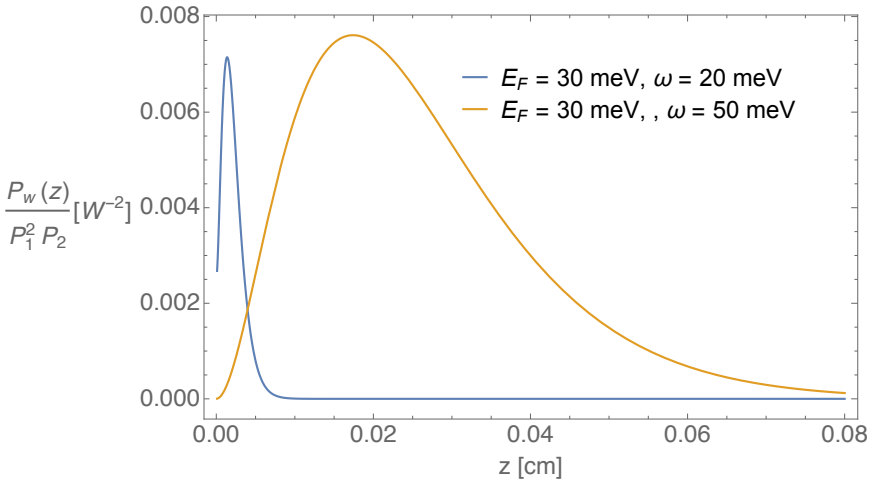

Figure 2.8: The nonlinear signal power as a function of distance z into the sample at two different frequencies and the same Fermi energy. Reprinted figure with permission of [44]

3. CONCLUSION

We studied the nonlinear optical response of Weyl semimetals within the kinetic equation approach which is valid at low enough frequencies in the vicinity of Weyl nodes and below the onset of interband transitions. We calculated the intensity of the nonlinear four-wave mixing signal in both transmission and reflection geometry. The doped bulk WSM exhibits extremely high third order nonlinearity combined with very high absorption loss. This led us to rethink the optimal strategies for nonlinear signal generation. The nonlinear signal intensity is maximized in the vicinity of bulk plasma resonance, which allows one to use ultrathin WSM films of the order of skin depth. The nonlinear generation efficiency turns out to be quite high for a thin film of a highly dissipative material: of the order of several mW per W3, in both transmission and reflection geometries. This could pave the way to interesting optoelectronic applications.

REFERENCES

[1] R.W. Boyd, *Nonlinear Optics* (Academic Press, London, 2003).

[2] P. A. Franken, A. E. Hill, C. W. Peters, and G. Weinreich Phys. Rev. Lett. 7, 118 (1961)

[3] Jia-Ming Liu. Nature Photonics volume 12, pages118–121(2018)

[4] J. A. Armstrong, N. Bloembergen, J. Ducuing, and P. S. Pershan Phys. Rev. 127, 1918

[5] P.A.M. Dirac, Proc. R. Soc. Lond. Ser. A 117, 610 (1928).

[6] H. Weyl, Proc. Natl. Acad. Sci. U. S. A. 15 (1929) 323.

[7] Kutayiah, A. Ryan. Nonlocal Nonlinear Optics In Graphene and the Optics of Weyl Semimetals. 2019. Texas A& M U, PhD dissertation.

[8] A. A. Burkov, Annu. Rev. Condens. Matter Phys. 9, 359 (2018).

[9] N. P. Armitage, E. J. Mele, and A. Vishwanath, Rev. Mod. Phys. 90, 015001 (2018).

[10] Imran, Muhammad. Theroy of Magnetotransport in The Dirac and Weyl Semimetas. 2020.University of Florida, PhD dissertation.

[11] Liu, Gerui. Nonlinear Optical Responses In Type-II Weyl Semimetals. 2019. University of Pennsylvania, PhD dissertation.

[12] A. A. Burkov, L. Balents, Phys. Rev. Lett. 107, 127205 (2011).

[13] X. Wan, A. M. Turner, A. Vishwanath, and S. Y. Savrasov, Phys. Rev. B 83, 205101 (2011).

[14] S.-Y. Xu et al., Science 349, 613 (2015).

[15] B. Q. Lv et al., Phys. Rev. X 5, 031013 (2015).

[16] A. A.Soluyanov et al., Nature 527, 495-498 (2015).

[17] B. Yan and C. Felser, Annu. Rev. Condens. Matter Phys. 8, 337 (2017).

[18] M. Z. Hasan, S.-Y. Xu, I. Belopolski, and S.-M. Huang, Annu. Rev. Condens. Matter Phys. 8, 289 (2017).

[19] M. Kargarian, M. Randeria, and N. Trivedi, Sci. Rep. 5, 12683 (2015).

[20] C. J. Tabert and J. P. Carbotte, Phys. Rev. B 93, 085442 (2016).

[21] J. Hofmann and S. Das Sarma, Phys. Rev. B 91, 241108 (2015).

[22] G. M. Andolina, F. M. D. Pellegrino, F. H. L. Koppens, and M. Polini, Phys. Rev. B 97, 125431 (2018).

[23] M. S. Ukhtary, A. R. T. Nugraha, and R. Saito, J. Phys. Soc. Jpn. 86, 104703 (2017).

[24] S. Kimura, H. Yokoyama, H. Watanabe, J. Sichelschmidt, V. Sus, M. Schmidt, and C. Felser, Phys. Rev. B 96, 075119 (2017).

[25] O. V. Kotov and Yu. E. Lozovik, Phys. Rev. B 98, 195446 (2018).

[26] K. Halterman, M. Alidoust, and A. Zyuzin, Phys. Rev. B 98, 085109 (2018).

[27] H. Rostami and M. Polini, Phys. Rev. B 97, 195151 (2018).

[28] Q. Chen, A. R. Kutayiah, I. Oladyshkin, M. Tokman, and A. Belyanin, Phys. Rev. B 99, 075137 (2019).

[29] C. A. C. Garcia, J. Coulter, and P. Narang, https://arxiv.org/abs/1907.04348.

[30] Q. Chen, M. Erukhimova, M. Tokman, and A. Belyanin, Phys. Rev. B 100, 235451 (2019).

[31] I. D. Tokman, Q. Chen, I. A. Shereshevsky, V. I. Pozdnyakova, I. Oladyshkin, M. Tokman, and A. Belyanin, Phys. Rev. B 101, 174429 (2020).

[32] A. A. Burkov and L. Balents, Phys. Rev. Lett. 107, 127205 (2011).

[33] R. Okugawa and S. Murakami, Phys. Rev. B 89, 235315 (2014).

[34] C. K. N. Patel, R. E. Slusher, and P. A. Fleury, Phys. Rev. Lett. 17, 1011 (1966).

[35] P. A. Wolff and G. A. Pearson, Phys. Rev. Lett. 17, 1015 (1966).

[36] C. C. Wang and N. W. Ressler, Phys. Rev. 188, 1291 (1969).

[37] A. Capretti, Y. Wang, N. Engheta, and L. D. Negro, Opt. Lett. 40, 1500 (2015).

[38] M. Z. Alam, I. D. Leon, and R. W. Boyd, Science 352, 795 (2016).

[39] Z. Sun, D. N. Basov, M. M. Fogler, Phys. Rev. B 97, 075432 (2018)

[40] Y. Zhong et al., Physica B: Condensed Matter 555, 81–84 (2019)

[41] J. W. Zuber, T. Zhao, S. Gong, M. Hu, R. B. Zhong, C. Zhang , and S. G. Liu, Phys. Rev. B 101, 085307 (2020).

[42] Y. Wang, M. Tokman, and A. Belyanin, Phys. Rev. B 94, 195442 (2016).

[43] T. Jiang, V. Kravtsov, M. Tokman, A. Belyanin, and M. Raschke, Nature Nano 14, 838 (2019).

[44] S. Almutairi, Q. Chen, M. Tokman, and A. Belyanin, Phys. Rev. B 101, 235156, (2020)

[45] O. Reshef, I. D. Leon, M. Z. Alam, and R. W. Boyd, Nat. Rev. Mater. 4, 535 (2019).

[46] N. Kinsley and J. Khurgin, Opt. Mat. Express 9, 2793 (2019).

APPENDIX A

THIRD-ORDER NONLINEAR OPTICAL CONDUCTIVITIES

The kinetic equation with the simplest relaxation term has the form:

$$\frac{\partial f}{\partial t} + v_F(\mathbf{n}\cdot\nabla)f - [e\mathbf{E} + \frac{v_F}{c}(\mathbf{n}\times\mathbf{B})]\cdot\frac{\partial f}{\partial \mathbf{p}} = \gamma[F(p) - f], \tag{A.1}$$

where $\mathbf{E}$ and $\mathbf{B}$ are external electric and magnetic fields, respectively, e is the electron charge, γ is the electron relaxation rate, $F(p)$ is an unperturbed (zeroth-order) distribution, which is chosen as the equilibrium Fermi-Dirac distribution, and f is the non-equilibrium distribution function. We consider the following form of the incident optical field:

$$\widetilde{\mathbf{E}}(x,t) = \sum_n \mathbf{E}_n(x,\omega_n)e^{-i\omega_n t} = \sum_n \mathbf{A}_n e^{ik_n x - i\omega_n t}, \tag{A.2}$$

and write the non-equilibrium distribution function f as

$$f = \sum_m \xi_m e^{iq_m x - i\omega_m t}. \tag{A.3}$$

where we have set $\xi_0 = F(p), E_0 = 0, \omega_0 = 0$. Because both the $\widetilde{\mathbf{E}}(x,t)$ and the f are real, i.e. $\widetilde{\mathbf{E}}(z,t) = \widetilde{\mathbf{E}}(z,t)^*$and $f = f^*$, we have $E_{-n} = E_n^*$, $\xi_{-n} = \xi_n^*$, $\omega_{-n} = -\omega_n$. Exploiting Eq.(A2) and Eq.(A3), Eq.(A1) becomes

$$\begin{aligned} & (\frac{\partial}{\partial t} + v_F\cos\phi\sin\theta\frac{\partial}{\partial x} + \gamma)f \\ = \;& \gamma F(p) + e[E_x\frac{\partial f}{\partial p_x} + E_y\frac{\partial f}{\partial p_y} + E_z\frac{\partial f}{\partial p_z}]. \end{aligned} \tag{A.4}$$

Transforming the Cartesian coordinate system to the spherical coordinate system, Eq.(A4) can

be rewritten as

$$
\begin{aligned}
& (\frac{\partial}{\partial t} + v_F \cos\phi \sin\theta \frac{\partial}{\partial x} + \gamma) f \\
= \;& \gamma F(p) + e[(E_x \cos\phi \sin\theta + E_y \sin\phi \sin\theta + E_z \cos\theta) \frac{\partial}{\partial p} \\
& + \frac{1}{p \sin\theta} (E_y \cos\phi - E_x \sin\phi) \frac{\partial}{\partial \phi} + \\
& \frac{1}{p} (E_x \cos\phi \cos\theta + E_y \sin\phi \cos\theta - E_z \sin\theta) \frac{\partial}{\partial \theta}] f. \qquad \text{(A.5)}
\end{aligned}
$$

Substituting Eq.(A2) and Eq.(A3) and setting $q_m = 0$, we obtain

$$
\begin{aligned}
& (-i\omega_n + \gamma) \xi_n \\
= \;& e[(E_{m,x} \cos\phi \sin\theta + E_{m,y} \sin\phi \sin\theta + E_{m,z} \cos\theta) \frac{\partial}{\partial p} \\
& + \frac{1}{p \sin\theta} (E_{m,y} \cos\phi - E_{m,x} \sin\phi) \frac{\partial}{\partial \phi} + \frac{1}{p} (E_{m,x} \cos\phi \cos\theta \\
& + E_{m,y} \sin\phi \cos\theta - E_{m,z} \sin\theta) \frac{\partial}{\partial \theta}] \xi_k, \qquad \text{(A.6)}
\end{aligned}
$$

where $\omega_n = \omega_m + \omega_k$. Now we define the operator $G^{n,m}(p, \phi, \theta)$ as

$$
\begin{aligned}
G^{n,m}(p, \phi, \theta) \;\equiv\; & g_1^{n,m}(\phi, \theta) \frac{\partial}{\partial p} + g_2^{n,m}(\phi, \theta) \frac{\partial}{p \partial \phi} \\
& + g_3^{n,m}(\phi, \theta) \frac{\partial}{p \partial \theta}, \qquad \text{(A.7)}
\end{aligned}
$$

where

$$
g_1^{n,m}(\phi, \theta) \equiv e \frac{E_{m,x} \cos\phi \sin\theta + E_{m,y} \sin\phi \sin\theta + E_{m,z} \cos\theta}{-i\omega_n + \gamma}, \qquad \text{(A.8)}
$$

$$
g_2^{n,m}(\phi, \theta) \equiv e \frac{E_{m,y} \cos\phi - E_{m,x} \sin\phi}{\sin\theta(-i\omega_n + \gamma)} \qquad \text{(A.9)}
$$

$$
\begin{aligned}
g_3^{n,m}(\phi, \theta) \;\equiv\; & (E_{m,x} \cos\phi \cos\theta + E_{m,y} \sin\phi \cos\theta - E_{m,z} \sin\theta) \\
& \times \frac{e}{(-i\omega_n + \gamma)}. \qquad \text{(A.10)}
\end{aligned}
$$

Thus the Eq.(A6) can be written as

$$\xi_n = \sum_{m,k} G^{n,m}\xi_k. \tag{A.11}$$

Solving in the linear approximation of the distribution function $\xi_n^{(1)}$, we get

$$\xi_n^{(1)} = G^{n,n}\xi_0 = g_1^{(n,n)}\frac{\partial F}{\partial p}, \tag{A.12}$$

for all possible ω_m and ω_k satisfying the relation $\omega_n = \omega_m + \omega_k$. For $\omega_n = \pm\omega_1, \omega_2, \omega_3$, we have $\omega_m = \pm\omega_1, \omega_2, \omega_3$ and $\omega_k = 0$. Solving for the second-order approximation of the distribution function $\xi_l^{(2)}$ with the second order frequency $\omega_l = \omega_m + \omega_k$, we get

$$\xi_l^{(2)} = \sum_{m,k} G^{l,m}\xi_k^{(1)} = \sum_{m,k} G^{l,m}G^{k,k}\xi_0, \tag{A.13}$$

for all possible ω_m and ω_k satisfying the relation $\omega_l = \omega_m + \omega_k$. For ω_l, we have $\omega_m = \pm\omega_1, \omega_2, \omega_3$ and $\omega_k = \pm\omega_1, \omega_2, \omega_3$. Solving for the third-order approximation of the distribution function $\xi_i^{(3)}$ with the frequency $\omega_i = \omega_j + \omega_l = \omega_j + \omega_m + \omega_k$, we get

$$\xi_i^{(3)} = \sum_{j,m,k} G^{i,j}\xi_l^{(2)} = \sum_{j,m,k} G^{i,j}G^{l,m}G^{k,k}\xi_0, \tag{A.14}$$

for all possible ω_j, ω_m and ω_k satisfying the relation $\omega_i = \omega_j + \omega_m + \omega_k$.

Now we study the expression $G^{(n_3,m_3)}G^{(n_2,m_2)}g_1^{(n_1,m_1)}\frac{\partial F}{\partial p}$. Firstly, by acting $G^{(n_2,m_2)} = G^2$ on the $g_1^{(n_1,m_1)}\frac{\partial F}{\partial p} = g_1^1\frac{\partial F}{\partial p}$, we have

$$G^2 g_1^1\frac{\partial F}{\partial p} = g_1^2 g_1^1\partial_{p^2}^2 F + g_2^2\partial_\phi g_1^1\frac{\partial_p F}{p} + g_3^2\partial_\theta g_1^1\frac{\partial_p F}{p}. \tag{A.15}$$

Secondly, acting $G^{(n_3,m_3)}=G^3$ on Eq.(A15), we have

$$\begin{aligned} G^3G^2g_1^1\frac{\partial F}{\partial p} &= (g_1^3\partial_p+g_2^3\frac{\partial_\phi}{p}+g_3^3\frac{\partial_\theta}{p}) \\ &\times(g_1^2g_1^1\partial_{p^2}^2F+\sin^2\theta g_2^2g_2^1\frac{\partial_pF}{p} \\ &+g_3^2g_3^1\frac{\partial_pF}{p}). \end{aligned} \tag{A.16}$$

Using the Eq.(A16) to evaluate the integral $I_i^{3,2,1}$, we obtain

$$\begin{aligned} I_i^{3,2,1} &= -ev_F\int_0^\infty\int_0^{2\pi}\int_0^\pi G^3G^2g_1^1\frac{\partial F}{\partial p}\times \\ &\begin{pmatrix}\cos\phi\sin\theta\\ \sin\phi\sin\theta\\ \cos\theta\end{pmatrix}p^2\sin\theta d\theta d\phi dp \\ &= \frac{8\pi e^4v_FF(0)}{15(\gamma-i\omega_1)(\gamma-i(\omega_1+\omega_2))} \\ &\times\frac{\Delta_{ijkl}E_1^jE_2^kE_3^l}{(\gamma-i(\omega_1+\omega_2+\omega_3))} \end{aligned} \tag{A.17}$$

where $\Delta_{ijkl}=\delta_{ij}\delta_{kl}+\delta_{ik}\delta_{jl}+\delta_{il}\delta_{jk}$. Here δ_{ij} is the Kronecker delta defined as $\delta_{ij}=1$ for $i=j$, $\delta_{ij}=0$ for $i\neq j$. Here we have used the relations $\int_0^\infty\frac{\partial F(p)}{p^2\partial p}p^2dp=-\int_0^\infty\frac{\partial^2F(p)}{p\partial p^2}p^2dp=-F(0)$ and $\int_0^\infty\frac{\partial^3F(p)}{\partial p^3}p^2dp=-\int_0^\infty\frac{\partial\left(\frac{\partial F(p)}{p\partial p}\right)}{\partial p}p^2dp=-2F(0)$.

Therefore, the nonlinear current $\mathbf{j}^{(\omega_n=\omega_1+\omega_2+\omega_3)}$ is then given by

$$\begin{aligned} \begin{pmatrix}j_x^{\omega_n}\\ j_y^{\omega_n}\\ j_z^{\omega_n}\end{pmatrix} &= -ev_F\int_0^\infty\int_0^{2\pi}\int_0^\pi\xi_n^{(3)}\begin{pmatrix}\cos\phi\sin\theta\\ \sin\phi\sin\theta\\ \cos\theta\end{pmatrix}p^2dpd\Omega \\ &= \frac{1}{3!}\left(I_i^{3,2,1}+Permutation(\omega_1,\omega_2,\omega_3)\right), \end{aligned} \tag{A.18}$$

where $d\Omega=\sin\theta d\theta d\varphi$ is the solid angle and $\xi_n^{(3)}$ is the third-order approximation of non-equilibrium distribution function associated with the third-order frequency $\omega_n=\omega_1+\omega_2+\omega_3$.

For a strongly Fermi-degenerate distribution we can replace the equilibrium distribution function with its zero-temperature limit, $F(p) = F(0)\Theta\left(p_F - p\right)$, where $F(0) = \frac{g_s g_w}{(2\pi\hbar)^3}$. Here g_s and g_w are the spin and Weyl node degeneracy, respectively. In this case, Eq.(A18) becomes

$$\begin{pmatrix} j_x^{\omega_n} \\ j_y^{\omega_n} \\ j_z^{\omega_n} \end{pmatrix} = \sigma_{ijkl} E_1^j E_2^k E_3^l, \tag{A.19}$$

where

$$\begin{aligned} & \sigma_{ijkl} \\ = \; & \frac{1}{3!}\Big(\frac{8\pi e^4 v_F g_s g_w \Delta_{ijkl}}{15(2\pi\hbar)^3(\gamma - i\omega_1)} \times \\ & \frac{1}{\left[\gamma - i(\omega_1+\omega_2)\right]\left[\gamma - i(\omega_1+\omega_2+\omega_3)\right]} \\ & + Permutation(\omega_1, \omega_2, \omega_3)\Big), \end{aligned} \tag{A.20}$$

is the third-order nonlinear optical conductivity at zero temperature.